6 Effective Interactions for Large-Scale Simulations of Complex Fluids

Jean-Pierre Hansen[1] and Hartmut Löwen[2]

[1] Department of Chemistry, Lensfield Road, Cambridge CB2 1EW, UK
[2] Institut für Theoretische Physik II, Heinrich-Heine-Universität Düsseldorf, Universitätsstraße 1, D-40225 Düsseldorf, Germany

Abstract. The simulation of complex fluids naturally involves widely different length scales. Integrating out parts of the microscopic degrees of freedom leads to the concept of effective interactions and provides a "coarse-grained" picture which can be simulated much more efficiently than a full microscopic model. This approach bridges length scales in complex fluids. In this chapter, we justify this procedure on a Statistical Mechanics level and apply it to a variety of different systems ranging from charged colloidal dispersions and polymer solutions (including star polymers and dendrimers) to mixtures of colloids and polymers and binary colloidal mixtures. Problems arising when this concept is transferred to nano-scales are pointed out. Finally the much harder problem of bridging different time scales in complex fluids is briefly discussed.

6.1 Introduction

While early Monte Carlo (MC) and Molecular Dynamics (MD) methods were historically designed to simulate simple fluids, represented, e.g., by the hard sphere or Lennard-Jones models, these agorithms are ill adapted to deal with fluids of increasing complexity, or "soft matter", because of the simultaneous presence of widely different length and time scales. Consider for example dispersions of spherical (e.g. polystyrene balls), rod-like (e.g. the "tobacco mosaic virus", TMV) or lamellar (e.g. clay) charge-stabilized colloidal particles in water. There are at least three length scales: the microscale of the solvent molecules, the nanoscale of the width of the electric double-layers formed by the co- and counterions (approximately equal to the Debye screening length), and the mesoscale of the colloidal particles (typically hundreds of nanometers). There are at least as many relevant time scales (although they are not always as clearly separated), and direct simulations based on a femtosecond time scale, or MC trial moves over molecular distances, are clearly inadequate to describe large scale phenomena over times of milliseconds and over distances of several microns. Returning to the case of charged colloids, the practical limit of "brute force" approaches, even neglecting the molecular nature of water (replaced by a dielectric continuum) is a total charge of less than $100e$ per polyion [1].

In this chapter we describe systematic coarse-graining procedures which lead to effective interactions between the largest, mesoscopic particles in mul-

ticomponent, multiscale fluid mixtures. These effective interactions follow from a rigorous "tracing out" of microscopic degress of freedom, and can be used in standard MC or MD simulations of samples involving only the large particles which now play the role of molecules in atomistic simulations. After a formal Statistical Mechanics justification of the coarse-graining procedure in Sect. 6.2, it will be successively applied to interacting electric double-layers (Sect. 6.3), to polarizable dielectric media (Sect. 6.4), to solutions of linear polymers (Sect. 6.5), star polymers and dendrimers (Sect. 6.6), to colloid-polymer (Sect. 6.7) and binary colloid mixtures (Sect. 6.8). In Sect. 6.9 the new challenges of coarse-graining nanoscale rather than mesoscale colloidal systems will be briefly considered, with biomolecular (e.g. protein) solutions in mind. Some conclusions will be drawn in Sect. 6.10.

It is worth stressing that this chapter will deal almost exclusively with the bridging of length scale gaps in complex fluids. The problem of how to cope with widely different time scales is far more difficult for supramolecular systems, and the corresponding methodology is still in its infancy.

6.2 Efficient Coarse-Graining Through Effective Interactions

An efficient statistical description of multi-component systems involving particles of widely different sizes requires a controlled-coarse-graining which may be achieved by integrating ("tracing") out the degrees of freedom of the majority components of "small" particles, which may be solvent molecules, microscopic ions ("micro-ions") or monomers of macro-molecules. For the sake of simplicity, consider an asymmetric binary "mixture" of N_1 "large" spherical particles, with centres of positions $\{\boldsymbol{R}_i\}$ $(1 \le i \le N_1)$, and $N_2 \gg N_1$ "small" particles at positions $\{\boldsymbol{r}_j\}$ $(1 \le j \le N_2)$. Restriction will be made to thermodynamic equilibrium states. If classical statistics apply, integration over momenta is trivial, and the focus will be on configurational averages. The total potential energy of the mixture may be conveniently split ino three terms:

$$U(\{\boldsymbol{R}_i\},\{\boldsymbol{r}_j\}) = U_{11}(\{\boldsymbol{R}_i\}) + U_{22}(\{\boldsymbol{r}_j\}) + U_{12}(\{\boldsymbol{R}_i\},\{\boldsymbol{r}_j\}) \tag{6.1}$$

At a fixed inverse temperature $\beta = 1/k_BT$, the configurational part of the Helmholtz free energy F of the two-component system may be formally expressed as:

$$\begin{aligned}
\exp(-\beta F) &= Tr_1\, Tr_2\, \exp(-\beta U) \\
&= Tr_1\, \exp(-\beta U_{11})\, Tr_2\, \exp(-\beta(U_{12}+U_{22})) \\
&= Tr_1\, \exp(-\beta U_{11})\, \exp(-\beta F_2(\{\boldsymbol{R}_i\})) \\
&= Tr_1\, \exp(-\beta V_{11}(\{\boldsymbol{R}_i\}))
\end{aligned} \tag{6.2}$$

where the short-hand trace notation implies integration over the configuration space of species 1 or 2, i.e.

$$Tr_\alpha = \frac{1}{N_\alpha!}\int d^{3N_\alpha} r$$

$V_{11}(\{\boldsymbol{R}_i\})$, the effective interaction energy of the large particles, is the sum of their direct (or bare) interaction energy U_{11}, and of the configurational free energy of the fluid of small particles in the "external" field of the large particles F_2; the latter depends parametrically on the configuration $\{\boldsymbol{R}_i\}$ of the large particles:

$$V_{11}(\{\boldsymbol{R}_i\}) = U_{11}(\{\boldsymbol{R}_i\}) + F_2(\{\boldsymbol{R}_i\}) \tag{6.3}$$

Up to now, no approximation has been made. If the large particles are fixed in a given configuration, (6.3) provides the exact energy from which the direct-configurational forces between the large particles can be derived. Once these particles move under the action of these effective forces, friction forces due to exchange of momentum with the bath of small particles will set in, and hydrodynamic forces due to induced flow of the latter will come into play. This difficult problem of hydrodynamic interactions [2] is not the subject of the present paper, which is restricted to static equilibrium properties independent of velocity-dependent forces.

Two key aspects of the effective interaction V_{11} must be underlined. Firstly, due to the presence of a free energy, F_2, V_{11} is obviously state-dependent, and has an entropic contribution of the small particles ($F_2 = U_2 - TS_2$). Secondly, although the direct interaction U_{11} may be pair-wise additive, this is no longer true of V_{11}. The free energy $F_2(\{\boldsymbol{R}_i\})$ generally has many-body-contributions, so that V_{11} will be of the more general form (with the change of notation $N_1 \to N$ and $V_{11} \to V_N$):

$$V_N(\{\boldsymbol{R}_i\}) = V_N^{(0)} + \sum\sum_{i\le j} v_2(\boldsymbol{R}_i,\boldsymbol{R}_j) + \sum\sum\sum_{i\le j\le k} v_3(\boldsymbol{R}_i,\boldsymbol{R}_j,\boldsymbol{R}_k) + \ldots . \tag{6.4}$$

$V_N^{(0)}$ is a state dependent but configuration-independent "volume" term, which has no bearing on the local structure of the large particles, but through its contribution to the thermodynamic properties, it can, in some cases, strongly influence their phase behaviour [3].

Expression (6.3) for the effective interaction, or potential of mean force, was derived in the canonical ensemble, where the total numbers of small and large particles are fixed (closed system). In many practical situations the binary system is in osmotic equilibrium with a pure phase of the small particles (e.g the solvent), and the appropriate ensemble for such an open system is the semi-grand canonical ensemble where N_1 and the chemical potential μ_2 of the small particles (rather than N_2) are fixed. The corresponding thermodynamic potential is the semi-grand potential $\Omega_2 = \Omega_2(T, N_1, \mu_2; \boldsymbol{R}_i)$, and

the effective interaction energy of the large particles will then be:

$$V_{11}(\boldsymbol{R}_i) = U_{11}(\boldsymbol{R}_i) + \Omega_2(\{\boldsymbol{R}_i\}) \tag{6.5}$$

which will again be state-dependent, a function of temperature, volume V and μ_2 (rather than $\rho_2 = N_2/V$).

In summary, the initial two-component system, involving a large number of microscopic degrees of freedom, has been reduced to an effective one-component system involving only the degrees of freedom of the mesoscopic particles. The price to pay is that the effective interaction energy is state-dependent and generally involves many-body terms. Approximations must now be invoked to calculate the highly non-trivial F_2 or Ω_2 term, i.e. the part of the interaction energy between the large particles induced by the small particles. Three different strategies have so far been used in practical implementations:

a) For any given configuration $\{\boldsymbol{R}_i\}$ of the large particles, the small particles are subjected to the "external" potential $U_{12}(\{\boldsymbol{R}_i\}, \{\boldsymbol{r}_j\})$, and hence form an inhomogeneous fluid, characterized by a local density $\rho(\boldsymbol{r}; \{\boldsymbol{R}_i\})$. The thermodynamic potentials F_2 or Ω_2 are functionals of $\rho(\boldsymbol{r})$, and full use can be made of the classical density functional theory (DFT) of non-uniform fluids to obtain tractable forms of F_2 or Ω_2 [4]. Given a form of $\Omega_2[\rho^*(\boldsymbol{r})]$, where $\rho^*(\boldsymbol{r})$ is a properly parametrized trial density, the equilibrium density follows from the variational principle:

$$\left.\frac{\delta\Omega_2[\rho^*(\boldsymbol{r})]}{\delta\rho^*(\boldsymbol{r})}\right|_{\rho^*=\rho} = 0 \tag{6.6}$$

Substitution of the optimum $\rho(\boldsymbol{r})$ into Ω_2 yields the equilibrium grand potential for any configuration $\{\boldsymbol{R}_i\}$. The optimization (6.6) may be implemented by steepest descent or conjugate gradient techniques, and the resulting effective potential energy between large particles can then be used directly in standard MC or MD simulations [5]. In the latter case, the forces $\boldsymbol{F}_i$ acting on the large particles may be directly calculated from a classical version of the Hellmann-Feynman theorem:

$$\begin{aligned}\boldsymbol{F}_i &= -\boldsymbol{\nabla}_i V_{11}(\{\boldsymbol{R}_j\}) \\ &= -\boldsymbol{\nabla}_i U_{11}(\{\boldsymbol{R}_j\}) - \langle \boldsymbol{\nabla}_i U_{12}(\{\boldsymbol{R}_j\}, \{\boldsymbol{r}_l\})_{\{\boldsymbol{R}_j\}}\end{aligned} \tag{6.7}$$

where the angular bracket denotes an equilibrium average over the degrees of freedom of the small particles, for a fixed configuration $\{\boldsymbol{R}_i\}$ of the large ones. If the interaction energy U_{12} between the two species is pairwise additive ($U_{12} = \sum_{i=1}^{N_1}\sum_{j=1}^{N_2} u_{12}(|\boldsymbol{r}_i - \boldsymbol{R}_j|)$), the force $\boldsymbol{F}_i$ is directly expressible in terms of the local density $\rho(\boldsymbol{r})$:

$$\boldsymbol{F}_i = -\boldsymbol{\nabla}_i U_{11}(\{\boldsymbol{R}_j\}) - \int \rho(\boldsymbol{r})\, \boldsymbol{\nabla}_i u_{12}(\boldsymbol{r} - \boldsymbol{R}_i)\, d\boldsymbol{r} \tag{6.8}$$

The optimization can also be achieved "on the fly", along lines directly inspired by the Car-Parrinello method for ion-electron systems [6]. Successive minimization and large particle updating steps are replaced by a single dynamical evolution, which involves the physical motion of the large particles and fictitious dynamics of the local density of small particles, parametrized by a plane wave expansion [7].

b) The previous DFT optimization method calculates directly the total effective energy of interaction between the large particles, or the resulting forces acting on each of these particles, without dividing V_N up into pair, triplet and higher order interactions, as written in (6.4). Another strategy is to attempt to compute these various contributions separately. At very low concentration of large particles, the effective pairwise interaction v_2 is expected to be dominant. In order to map out v_2 as a function of the distance r between two large particles, one may use standard MC or MD algorithms to simulate a bath of small particles in the field of two fixed large particles. Equation (6.7) may then be used to calculate the mean forces acting on the two mesoparticles (which are opposite if the latter are identical) for each distance $r = |\boldsymbol{R}_1 - \boldsymbol{R}_2|$. The effective pair potential $v_2(r)$ finally follows from an integration of the forces. This procedure must be repeated for each distance r, but there are no time-scale or ergodicity problems, since the two large particles are fixed. The same goal can be achieved by appealing once more to DFT for the inhomogeneous fluid of small particles, subjected to the force field of two fixed large particles. The optimization may be carried out in r-space, using an adequate Eucledian or non-Eucledian [8,9] grid on which the local density of small particles is defined. For two identical large particles, the local density has obvious cylindrical symmetry, but under favourable conditions, a considerable simplification occurs by fixing one of the large particles and considering an infinitely dilute solution of large particles in a bath of small particles around the fixed large particle. The density profile of the large particles in the zero concentration limit is directly related to the effective pair potential between two large particles in a bath of small particles [10], i.e.,

$$v_2(r) = -k_B T \lim_{\rho_1 \to 0} \ln\left(\frac{\rho_1(r)}{\rho_1(r \to \infty)}\right) \tag{6.9}$$

The advantage is that the two density profiles $\rho_1(r)$ and $\rho_2(r)$ are now spherically symmetric, but the method requires the prior knowledge of an accurate density functional for an asymmetric binary mixture. This strategy may be generalized to the calculation of three-body and higher order effective interactions, by considering the density profiles of large and small particles around two or more fixed large particles [11]. Applications of this strategy will be discussed in Sects. 6.5-6.8.

c) Although the effective interaction energy (6.3) or (6.5) is not, in general, pairwise additive at finite concentrations of the large particles, it would

be very convenient, for computational purposes, to reduce it, at least approximately, to a pairwise additive form. Contrarily to the two-body potential $v_2(r)$ discussed in the previous paragraph, which is only valid in the low density limit of large particles, the effective pair potential corresponding to finite concentrations is expected to be density-dependent, and will, in some average sense, incorporate the contributions of higher order terms in (6.4). Such effective density-dependent pair potentials can, in some cases, be derived from approximate functionals or from inversion procedures, examples of which will be described in Sect. 6.5.

6.3 Electric Double-Layers

Electric double-layers around mesoscopic colloidal particles of various shapes (spheres, rods, platelets, ...) or around polyelectrolytes make the generally dominant contribution to the effective interaction between highly-charged particles, which will be referred to as polyions [12,13]. Most simulations are based on a primitive model, whereby the discrete nature of the aqueous solvent is neglected, and a macroscopic value of the dielectric permittivity ϵ is assumed. At very low polyion concentration, strategy b) of the previous section may be adopted to compute an effective pair interaction between two polyions, which is screened by microscopic counterions of opposite sign, as well as coions in the presence of added salt. The resulting effective pair potential turns out to be invariably repulsive, of the screened Coulomb form predicted a long time ago by Derjaguin, Landau, Verwey and Overbeek (DLVO) [14] as long as the microions are monovalent. However if divalent counterions are present, they are more strongly correlated, and this may lead to a short-range attraction between equally-charged polyions, due to an overscreening effect [15]. Although most of the work on effective pair interactions has focussed so far on spherical polyions, some recent MC simulations have investigated the case of parallel lamellar colloids [16], and this work has very recently been extended to charged discs of various relative orientations [17]. The triplet interaction between spherical polyions has similarly been calculated by MD simulations of co and counterions in the field of three fixed polyions [18], and turns out to be attractive under most circumstances. In the opposite limit of high concentrations, each polyion is confined to a cage of neighbouring polyions, so that many-body interactions are expected to be important, and pairwise additivity of the effective interaction is expected to break down. It is then reasonable to consider a Wigner-Seiz cell model, where a cell of geometry adapted to the shape of the polyions (e.g. a spherical cell for spherical polyions) contains one polyion at its centre, surrounded by co and counterions, such that overall charge neutrality is ensured, and with appropriate boundary conditions for the electric field on the surface of the cell. A physically reasonable boundary condition is to impose that the normal component of the electric field vanishes on the surface. The initial problem

involving many polyions is thus approximately reduced to the much simpler problem of a single polyion surrounded by its electric double-layer. Although all information on correlations between polyions is lost, the cell model allows a calculation of the thermodynamic properties of concentrated suspension, from MC or MD simulations of the inhomogeneous fluid of microions contained in the cell, as well as an estimate of the effective polyions charge, taking into account the phenomenon of counterion "condensation" [19,20]. Such simulations provide stringent tests for approximate DFT calculations, including Poisson-Boltzmann (PB) theory.

At moderate polyion concentrations, the two previous strategies break down. Strategy a) of the previous section, based on the step by step or "on the fly" optimization of an appropriate free energy functional of the microion density profiles, is the most appropriate [7]. The free energy functional $F_2[\rho_+(\boldsymbol{r}), \rho_-(\boldsymbol{r}), \{\boldsymbol{R}_i\}]$ of the co- and counterion densities is conveniently split into ideal, Coulomb, external and correlation parts:

$$F_2[\rho_+, \rho_-] = F_{id}[\rho_+] + F_{id}[\rho_-] + F_{Coul}[\rho_c] + F_{ext}[\rho_+] + F_{ext}[\rho_-] + F_{corr}[\rho_+, \rho_-] \tag{6.10}$$

where:

$$F_{id}[\rho_\alpha] = k_B T \int \rho_\alpha(\boldsymbol{r}) \left[\ln(\Lambda_\alpha^3 \rho_\alpha(\boldsymbol{r})) - 1\right] d\boldsymbol{r} \tag{6.11}$$

$$F_{Coul}[\rho_\alpha] = \frac{e^2}{2} \int d\boldsymbol{r} \int d\boldsymbol{r}' \frac{\rho_c(\boldsymbol{r})\, \rho_c(\boldsymbol{r}')}{|\boldsymbol{r} - \boldsymbol{r}'|} \tag{6.12}$$

$$F_{ext}[\rho_\alpha] = \int \varphi_{ext}(\boldsymbol{r})\, \rho_\alpha(\boldsymbol{r})\, d\boldsymbol{r} = \sum_{i=1}^{N_1} \int u_{1\alpha}(\boldsymbol{r} - \boldsymbol{R}_i)\, \rho_\alpha(\boldsymbol{r})\, d\boldsymbol{r} \tag{6.13}$$

In (6.12), $\rho_c(\boldsymbol{r}) = z_+\rho_+(\boldsymbol{r}) + z_-\rho_-(\boldsymbol{r})$ is the charge density of the microions (of valences z_α). The polyion-microion potentials $u_{1\alpha}$ in (6.13) contain a hard core repulsion and a long-range Coulomb attraction (counterions) or repulsion (coions). Rapid variations of the densities profiles $\rho_\alpha(\boldsymbol{r})$ near the surfaces of the polyions, which would pose numerical problems in r-space (grid) or k-space (large $\boldsymbol{k}$ Fourier components) may be avoided by the use of appropriate classical polyion-microion pseudopotentials [7]. The correlation term F_{corr} may be expressed within the local density approximation (LDA) [7]. If it is neglected, the functional (6.10) reduces to the mean-field Poisson-Boltzmann (PB) form. Optimization based on the functional (6.10-6.13) has been achieved with the "on the fly" MD strategy for spherical polyions with

counterions only (no salt) [7], and in the presence of salt (i.e. with co and counterions) [21]. The effective forces between colloids are reasonably well represented by a pair-wise additive screened-Coulomb form provided the (effective) polyion charge and the screening length are treated as adjustable parameters. Other applications include rigid rod-like polyions [22], and flexible polyelectrolytes [5], the latter being investigated by MC simulations coupled with steepest descent optimization, to allow a more efficient exploration of polyelectrolyte configuration space. If F_{corr} is neglected in the functional (6.10), and the ideal terms are replaced by their quadratic expansion in powers of $\Delta\rho_\alpha(\boldsymbol{r}) = \rho_\alpha(\boldsymbol{r}) - \rho_\alpha$ (where ρ_α is the bulk concentration of microions), the total functional is quadratic in the $\rho_\alpha(\boldsymbol{r})$, and the Euler-Lagrange equations resulting from the extremum conditions (6.6) can be solved analytically [7]. The resulting total effective energy of the polyions is then strictly pairwise additive, and the effective pair potentials are of the linearly screened DLVO form. The entire procedure is justified only for relatively weak microion inhomogeneities (i.e. $|\Delta\rho_\alpha(\boldsymbol{r})|/\rho_\alpha < 1$), i.e. for low absolute polyion valence $|Z_p|$. If the polyion charge is distributed over a number ν of interaction sites, each carrying a charge $Z_p\, e/\nu$, linear screening may be an adequate approximation for each interaction site. The resulting "Yukawa site" model, where all sites on neighbouring particles interact via a screened Coulomb (or Yukawa) pair potential, has been used to simulate charged rods [22] or charged discs representing clay particles [23].

An excellent literature survey of the recent simulation work on charged-stabilized colloidal suspensions is provided by the review of M. Dijkstra [24].

6.4 Simulating the Polarization of Dielectric Media

The coarse-graining methods developed for poly-ionic systems may be extended to take into account the polarization of dielectric media. This is important when dealing with mesoscopic interfaces, or the solvation of highly charged macromolecules of biological interest, like DNA or proteins, by water [25]. Since a full molecular description of the solvent surrounding the macromolecules would be computationally prohibitive, water is generally treated as a dielectric continuum which is polarized by the charge distribution on the macromolecules. The key problem is to determine the spatially varying polarization $\boldsymbol{P}(\boldsymbol{r})$ induced in the dielectric, for any configuration of the "external" charges carried by the macromolecules and counter- and coions and to calculate the resulting electrostatic potential $\Psi(\boldsymbol{r})$, due to the external and induced polarization charges.

Electrostatic problems involving dielectric polarization can be solved variationally, as in the case of electric double-layers considered in the previous section, by minimizing an appropriate functional F of the polarization density $\boldsymbol{P}(\boldsymbol{r})$ [26] or of the polarization charge [27]

$$\rho_{pol}(\boldsymbol{r}) = -\boldsymbol{\nabla}\cdot\boldsymbol{P}(\boldsymbol{r}) = \boldsymbol{\nabla}\cdot[\chi(\boldsymbol{r})\boldsymbol{\nabla}\Psi(\boldsymbol{r})] \tag{6.14}$$

where $\chi(\boldsymbol{r})$ is the local dielectric susceptibility. The non-linear nature of the problem is immediately apparent from the self-consistency requirement which links $\Psi(\boldsymbol{r})$ to $\rho_{pol}(\boldsymbol{r})$:

$$\Psi(\boldsymbol{r}) = \Psi_0(\boldsymbol{r}) - \int \frac{\rho_{pol}(\boldsymbol{r}')}{|\boldsymbol{r}-\boldsymbol{r}'|} d\boldsymbol{r} \tag{6.15}$$

where $\Psi_0(\boldsymbol{r})$ is the "external" electrostatic potential, due to the charge distribution on the macromolecules. The advantage of using $\boldsymbol{P}(\boldsymbol{r})$ as a variational field is that an electrostatic free energy functional can be constructed in the form [28,29]

$$\begin{aligned} F_{el}[\boldsymbol{P}(\boldsymbol{r})] = \; & \frac{1}{2}\int \Psi_0(\boldsymbol{r})\rho(\boldsymbol{r})d\boldsymbol{r} \\ & + \frac{1}{2}\int |\boldsymbol{P}(\boldsymbol{r})|^2/\chi(\boldsymbol{r})d\boldsymbol{r} - \int \Psi_0(\boldsymbol{r})\boldsymbol{\nabla}\cdot\boldsymbol{P}(\boldsymbol{r})d\boldsymbol{r} \\ & + \frac{1}{2}\int\int \frac{(\boldsymbol{\nabla}\cdot\boldsymbol{P}(\boldsymbol{r}))(\boldsymbol{\nabla}'\cdot\boldsymbol{P}(\boldsymbol{r}'))}{|\boldsymbol{r}-\boldsymbol{r}'|} d\boldsymbol{r}\, d\boldsymbol{r}' \end{aligned} \tag{6.16}$$

Minimization of (6.16) with respect to $\boldsymbol{P}(\boldsymbol{r})$, for a fixed macromolecular configuration (and hence $\Psi_0(\boldsymbol{r})$), leads back to the usual constitutive equations of electrostatics, and the value of F_{el} at the minimum coincides with the standard expression for the electrostatic energy of a polarizable medium in an external field. This functional has been used by Marchi et al. in MD simulations of polypeptides, with an "on the fly" optimization strategy [26].

A functional of the polarization charge (6.14), rather than of the polarization itself can be constructed, which upon minimization, leads back to the standard relations of electrostatics [30]. At its minimum, this functional reduces to minus the electrostatic energy, so that it cannot be used in an obvious way in dynamical optimization algorithms, but working with $\rho_{pol}(\boldsymbol{r})$, rather than with $\boldsymbol{P}(\boldsymbol{r})$, has two advantages. First a scalar rather than a vectorial field is to be handled on a grid. But more importantly, if the interface between dielectrics is sharp, so that the susceptibility is essentially a step function, the polarization charge (6.14) reduces to a surface charge which may be defined on a 2d (rather than full 3d) grid, resulting in considerable computational savings. In MD or MC simulations of macromolecular charge distributions near interfaces, the polarization charge is efficiently calculated by a steepest descent algorithm on a step by step basis. The method has been successfully tested for simple model systems [30], and is at present being applied to the simulation of ion channels through membranes, where the channel protein and the embedding lipid bilayer are treated as a dielectric continuum responding to the moving electric charges on the cations and on the water molecules [31]. Note that the role of the macromolecule and of water are inverted compared to the macromolecular hydration problem [27,26].

6.5 Coarse-Graining Linear Polymer Solutions

A solution of linear polymers involves many different length scales ranging from microscopic bond length over the persistence length and the radius of gyration (coil size) to the mean-inter coil distance, see Fig. 6.1. Therefore, the direct simulation of on or off-lattice models of polymer solutions or melts are very computer-intensive [32], because even the simplest linear polymers involve thousands of monomers. Even if the latter are grouped into Kuhn segments, corresponding to one persistence length, the system will involve a very large number of linearly connected, interacting particles. If N is the number of polymer coils, each made up of M segments, the total number of degrees of freedom is $3NM$ which is a factor of M ($\gg 1$) larger than for simple fluids or rigid colloidal particles, assuming that the organic or aqueous (for polyelectrolytes) solvent is replaced by a continuum. The question hence naturally arises of how to coarse-grain the initial, fully microscopic model involving M monomers or segments per chain. The situation is somewhat different from the previously examined cases, involving large and small particles. The polymer case is more "democratic" in that all monomers play identical roles, at least in the scaling limit $M \to \infty$, where end effects become negligible. An old idea, which goes back at least to Flory [33] is to derive an effective interaction between the centres of mass (CM) of neighbouring polymer coils, by integrating over the individual monomer degrees of freedom of two or more coils, for fixed relative positions of their CM's. Consider first the case of two isolated polymer coils with monomer coordinates $\{\boldsymbol{r}_{i\alpha}\}_M$ ($i = 1, 2; 1 \leq \alpha \leq M$) and CM's:

$$\boldsymbol{R}_i = \sum_{\alpha=1}^{M} \boldsymbol{r}_{i\alpha} \tag{6.17}$$

If $U(\{\boldsymbol{r}_{i\alpha}\})$ is the total potential energy of interaction of all monomers, the probability distribution of the CM's is:

$$P(\boldsymbol{R}_1, \boldsymbol{R}_2) = \frac{1}{Q_{2M}} \int e^{-\beta U(\{\boldsymbol{r}_{i\alpha}\})} \prod_{i=1,2} \delta(\boldsymbol{R}_i - \sum_{\alpha} \boldsymbol{r}_{i\alpha}) \prod_{\alpha} d\boldsymbol{r}_{i\alpha} \tag{6.18}$$

where Q_{2M} is the corresponding configurational partition function (equal to the $6M$-dimensional integral in (6.18), without the δ-functions). By analogy with (6.2), the effective pair interaction between the CM's is then given by:

$$v_2(\boldsymbol{R}_1 \boldsymbol{R}_2) = -k_B T \ln[P(\boldsymbol{R}_1 \boldsymbol{R}_2)] \tag{6.19}$$

The effective potential will only depend on $r = |\boldsymbol{R}_1 - \boldsymbol{R}_2|$. $v_2(r)$ is expected to be of the order of the radius of gyration R_g of the polymers, since for $r \geq R_g$, there will be little overlap between two coils. Swollen polymers in good solvent (where $R_g \sim M^{\nu}$, with $\nu \simeq 0.6$, the Flory exponent) are highly fractal objects, i.e. the mean monomer density inside a coil $\sim M^{1-3\nu}$ goes to zero in the scaling limit. An immediate consequence is that $v_2(r)$ is

a "soft" potential, and that $v_2(r = 0)$ is finite [34], i.e. the polymer coils may be modelled as penetrable spheres. On and off-lattice simulations of self-avoiding walk (SAW) polymers [35,36], as well as renormalization group (RG) calculations for the continuous "thread" model [37], show that the pair potential $v_2(r)$ is well approximated by a single Gaussian:

$$\frac{v_2(r)}{k_B T} = \xi \exp(-J(r/R_g)^2) \tag{6.20}$$

where $J \simeq 1$; the simulations yield [36] for $M \to \infty$:

$$\xi \simeq 1.80 \pm 0.05 \tag{6.21}$$

while the RG yields the following $\epsilon = 4 - d$ expansion.

$$\xi = 0.94\epsilon + 0.62\epsilon^2 + O(\epsilon^3) \tag{6.22}$$

These results are independent of molecular detail, so that the simplest lattice models and most efficient MC sampling (e.g. the pivot algorithm) can be used to determine the effective interactions. Note that for self-avoiding walk (SAW) polymers (which involve only excluded volume interactions between monomers), the effective interaction is purely entropic in nature as signalled by the scaling with $k_B T$.

When nearest-neighbour attractions between monomers are included to allow for solvent conditions (strong attractions correspond to poor solvent), the effective pair potential between the CM's becomes less repulsive, and develops an attractive part as Θ-conditions are approached [35,38]. If ϵ_0 denotes the depth of the attraction, ergodicity problems become more and more severe in the simulations when $\epsilon_0 / k_B T > 1$, but can be overcome by using Bennett's overlapping distribution method [39,40]. Returning to the SAW model, appropriate for good solvent conditions, the method for determining the effective pair potential can be extended to effective three- and more-body interactions, by simulating three or more polymers for various configurations of their CM's [41]. The main qualitative results are that more-than-two body interactions alternate in sign (the three-body potential being mostly attractive), and that the absolute amplitudes of higher order interactions do appear to decrease with increasing order in line with scaling theory [42].

However the strategy of adding higher order effective interactions in simulations of polymer solutions of finite concentration is computationally inefficient. A much more efficient strategy is to determine state-dependent effective pair interactions by a systematic inversion procedure [36]. The pair distribution function $g(r)$ of the CM's of systems of SAW polymers at finite concentration is calculated by direct simulations of a few hundred polymers on a lattice, using efficient MC algorithms [40]. An effective concentration-dependent effective pair potential between the CM's is then determined by Ornstein-Zernike (OZ) inversion, assuming some adequate closure relation,

like the HNC closure [43]. In view of the softness of the resulting pair potential, HNC theory becomes asymptotically exact in the high concentration limit, and is extremely accurate at all concentrations [44,45]. The inversion is a noniterative, one-step procedure, and it has been proven that there is a one-to-one correspondence between any given $g(r)$ and a $v(r)$ (uniqueness theorem [46]). The resulting effective pair potentials turn out to be weakly dependent on concentration [36]. They may be used in large-scale simulations of polymer solutions, of polymers at interfaces or of colloid-polymer mixtures [47], to study, in particular, the effect of polymer interactions on the depletion force between colloidal particles [36,48]. In its original formulation, this coarse-graining strategy has one obvious drawback, namely that simulations of the full monomeric representation of polymer solutions are initially required to determine the CM pair contribution function $g(r)$, for each polymer concentration, a rather formidable task, even if the resulting effective potentials may then be used to explore a range of different large-scale phenomena. However even this drawback can be overcome by calculating the monomer-monomer pair distribution function within the accurate PRISM theory [49], and then extracting the CM pair distribution function from its monomeric counterpart, together with the form factor (or internal structure factor) of a single polymer coil, using a recently proposed, accurate relation between these three correlation functions [50].

6.6 Star Polymers and Dendrimers

The ideas of coarse-graining, as applied to solutions of linear polymer chains in the previous section, can be generalized to polymers with a more complicated architecture. We shall discuss solutions of star polymers and dendrimers in more detail. Star polymers [51] consist of f linear polymer chains which are chemically anchored to a common centre (f is called functionality or arm number). Obviously, linear polymers are a special case of star polymers when $f = 1, 2$ depending whether the end or middle segment is taken as "centre". Dendrimers, on the other hand, can be viewed as iterated star polymers: periodically, any linear chain branches off into n additional chains (n is called degree of branching) which is repeated g times (g is called generation number). For $f > 3$, in contrast to linear chains, star polymers and dendrimers possess a natural centre which serves as an appropriate statistical degree of freedom.

Let us first focus on *star polymers in a good solvent*. A full monomer-resolved computer simulation is completely out of reach of present-day computers: If N is the number of stars and M the number of monomers per chain, a total number of NfM particles has to be simulated, f times more than for a solution of linear chains and fM times more than for simple fluids. The strategy b) of Sect. 6.2, however, can be efficiently used to make progress. First consider only two stars at fixed separation r and average the force acting

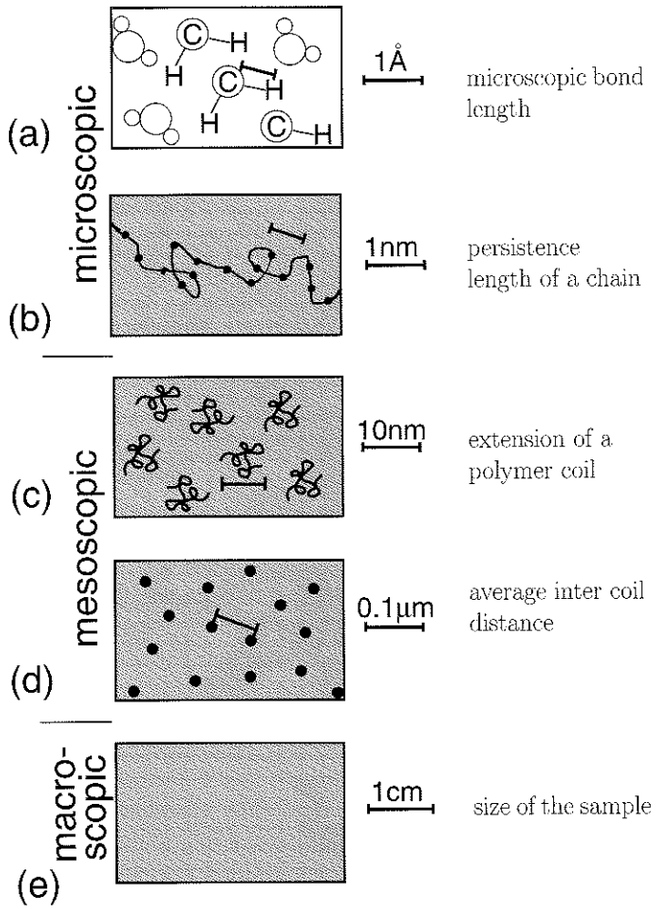

Fig. 6.1. Polymer solution on different length scales. (a): microscopic picture, water and hydrocarbon chains are shown, the chemical bonds have a range of typically 1Å. (b): On a larger scale, the persistence length of the chains is relevant. (c): the spatial extension σ of a single polymer coil. (d): all the coils are point particles on this scale governed by the mean intercoil distance (e): size of the macroscopic sample.

on their centres during an ordinary MC or MD simulation of the monomers. Such a simulation involves $2fM$ particles only. A typical simulation snapshot is shown in Fig. 6.2. This is repeated for different r. By integrating the distance-resolved data for the force, the effective interaction potential $v(r)$ is obtained. This interaction is repulsive, since the presence of another star reduces the number of configurations available to the chains. For small arm numbers $f \leq 10$, the simulation results confirm an effective pair potential of

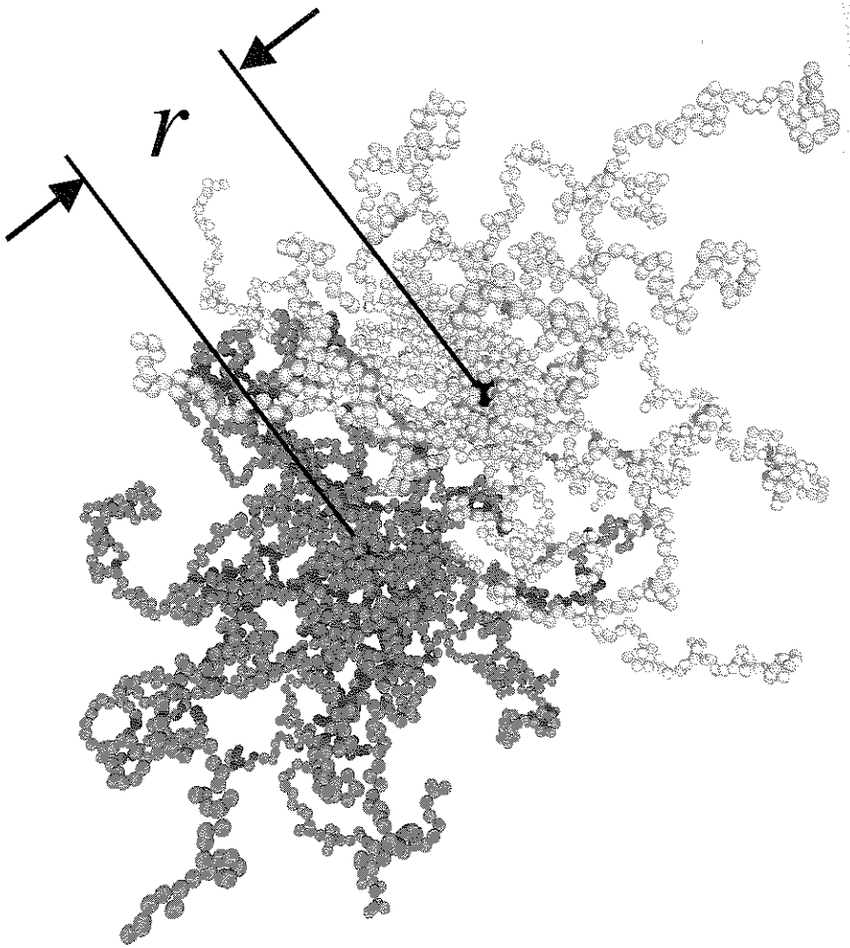

Fig. 6.2. Typical configuration for two stars with $f = 18$ and $M = 50$ monomers per chain as obtained from a snapshot during a Molecular Dynamics simulation with r denoting the distance between their centres. By courtesy of A. Jusufi.

the log-Gauss form:

$$v(r) = \frac{5}{18} k_{\rm B} T f^{3/2} \begin{cases} -\ln(\frac{r}{\sigma}) + \frac{1}{2\tau^2\sigma^2} & \text{for } r \le \sigma; \\ \frac{1}{2\tau^2\sigma^2} \exp\left(-\tau^2 \frac{r^2-\sigma^2}{\sigma^2}\right) & \text{for } r > \sigma, \end{cases} \tag{6.23}$$

where σ is the corona diameter of a single star measuring the spatial extent of the monomeric density. For large distances r, the interaction is Gaussian as for linear chains. It then crosses over, at the corona diameter of the star, to a logarithmic behaviour for overlapping coronae as predicted by scaling theory

[52] which implies a very mild divergence as $r \to 0^+$. The matching at $r = \sigma$ is done such that the force $-dv/dr$ is continuous. In (6.23) , $\tau(f)$ is known from a fit to computer simulation results; for $f = 2$ we obtain $\tau = 1.03$ in line with the Gaussian potential (6.20) used for linear chains.

For larger arm numbers, $f > 10$, on the other hand, a geometric blob picture of f cones around the star centre, each containing one linear chain is justified [53]. The effective force for nearly touching coronae decays exponentially with r, the associated decay length is the outermost blob-diameter $2\sigma/\sqrt{f}$. This motivates a log-Yukawa form of $v(r)$ [54]:

$$v(r) = \frac{5}{18} k_B T f^{3/2} \begin{cases} -\ln(\frac{r}{\sigma}) + \frac{1}{1+\sqrt{f}/2} & \text{for } r \le \sigma \\ \frac{\sigma}{1+\sqrt{f}/2} \frac{\exp(-\sqrt{f}(r-\sigma)/2\sigma)}{r} & \text{for } r > \sigma \end{cases} \tag{6.24}$$

again matched at the corona diameter $r = \sigma$ such that the force is continuous. This potential was verified in monomer-resolved simulations [55] for a large range of arm numbers.

Using scaling theory and monomer-resolved simulations of a triangular configuration of three stars [42], triplet interactions were shown to be negligibly small outside the corona and at most 11 percent of the pairwise forces for penetrating triplets inside the corona; consequently the effective pair-wise description for the many-body system is adequate provided the number density ρ_s of the stars is not much higher than the overlap density $1/\sigma^3$. Large scale simulations involving many stars were performed using the pair potential of (6.24) [56,57]. Due the crossover of $v(r)$ at $r = \sigma$ from a harsh Yukawa to a soft logarithmic behaviour, uncommon structural and thermodynamical properties were obtained. First, the main peak of the liquid structure factor changes non-monotonically with increasing density [57]. Secondly, the bulk phase diagram exhibits [56] a reentrant melting behaviour for $34 < f < 44$ and stable anisotropic crystal lattices. The latter finding has been supported by experiments [58].

Next let us briefly discuss *star polymers in a poor solvent.* The only work in this direction is close to the Θ-point where the chains are weakly interacting. Consequently the resulting effective repulsion is weaker than in good solvent. More quantitatively, an effective potential between two plates is available within a self-consistent field approach for polymers grafted on flat plates where the grafting density is high and the self-avoidance is weak [59]. This was extended to spherical particles by employing the Derjaguin approximation [60,61] providing an analytical expression for the effective pair potential $v(r)$. In the limit of small core sizes, this expression has been successfully tested against scattering data for $f = 64$ arm stars in a solvent close to Θ conditions [62]. What is still unexplored is a systematic approach for arbitrary solvent quality which continously switches between good solvent quality to the Θ point and beyond.

Much more stretched configurations are achieved for *polyelectrolyte stars* ("porcupines") due to the strong Coulomb repulsion of the charged monomers

along the chains. If one brings two polyelectrolyte stars together they hardly interdigitate but retract. A variational analysis [63] for the effective force, which includes Coulomb interactions and entropies of the counterions, reveals that the entropy of the counterions which are inside the coronae of the two polyelectrolyte stars dominates the interaction, confirming an old idea of Pincus [64]. The analytical theory was quantitatively verified by computer simulations with explicit monomers and counterions [63]. Inside the corona, the resulting effective force could be fitted by an inverse-power law $\propto r^{-\gamma}$ where the exponent γ slightly depends on the actual charging conditions but is always around $0.7 - 0.8$. By integration, an effective potential is obtained which stays finite at the origin and behaves inside the corona as $v(r) = v(0) - Cr^{1-\gamma}$ with a positive constant C. However, the actual value $v(0)$ for completely overlapping stars is much larger than k_BT so that significant overlap is rare. Due to the softness of the interaction, similar structural anomalies as obtained for star polymers are expected including a non-monotonic variation of the first peak in the structure factor for increasing density and reentrant melting.

Finally, *dendrimers* in a good solvent have been addressed. For a branching degree $b = 2$ and a generation number $g = 4$ an effective Gaussian potential can be derived theoretically [65], provided the centre-to-centre distance r is larger than the corona diameter σ. In formal analogy to linear polymer chains one obtains:

$$v(r) = B \exp(-r^2/\sigma^2) \tag{6.25}$$

The important difference from the case of linear polymer chains is that the prefactor

$$\frac{B}{k_BT} = \frac{M^2 v_0}{\pi^{3/2}\sigma^3} \tag{6.26}$$

is much larger than 1, with M denoting the total number of monomers per dendrimer and v_0 the excluded volume parameter per monomer. The Gaussian interaction (6.25) was confirmed quantitatively by scattering experiments [65]. A detailed comparison for $b = 2$ dendrimers with higher generation number $g = 5$ reveals that the effective potential $v(r)$ is well described by a sum of two Gaussians [66] comprising the effect of the stiff inner region and the floppy outer region of a dendrimer. The effect of increasing the degree of branching b is much less explored. In principle a Gaussian pair potential (6.25) (or a superposition of them) is again expected but the prefactor B/k_BT should grow with increasing b. Thereby it should be possible to tune the prefactor B/k_BT to larger values, where freezing is expected [67].

Coarse-graining star polymers and dendrimers thus maps them onto simple liquids with soft interactions (socalled mean-field fluids) which in turn implies peculiar properties. Hence the concept of effective interactions not only allows for efficient simulation, but also provides insight into the physical behaviour.

6.7 Colloids and Polymers: Depletion Interactions

If a sterically-stabilized colloidal particle is brought into a non-adsorbing polymer solution, the latter are depleted in a zone around the colloidal surfaces due to the colloid-polymer repulsion. The width of this zone is of the order of the radius of gyration $d_p/2$ of the polymers. If one now brings two colloidal particles close to each other, the two depletion zones overlap, which brings about a free energy gain of the polymers relative to a situation of non-overlapping zones, resulting in an effective attraction between the colloids, the so-called depletion attraction. Alternatively one can view the attraction arising from an unbalanced osmotic pressure exerted on the colloidal particles by the surrounding polymers.

The simplest model for colloid-polymer mixtures including the depletion effect is the so-called Asakura-Oosawa (AO) model [68] which assumes hard core interactions between the colloids of diameter d_c, further hard-core interactions between the polymers and the colloids with a range $(d_c + d_p)/2$, but no interaction at all between polymers. The ideality of the polymers is a crucial approximation which is fulfilled only for dilute polymer solutions, but it allows to investigate many of the statistical properties of the AO model analytically. For instance, the effective interaction $v(r)$ between a colloidal pair can be calculated to be the product of the polymer osmotic pressure $P_p = k_BT\rho_p$ and the overlap volume of the two depletion zones consisting of two spherical half-caps. Explicitly it reads

$$\frac{v(r)}{k_BT} = \begin{cases} \infty & \text{for } r \le d_c \\ \rho_p \frac{\pi}{6}(d_c + d_p)^3 \left[1 - \frac{3r}{2(d_c+d_p)} + \frac{1}{2}\frac{r^3}{(d_c+d_p)^3}\right] & \text{for } d_c < r \le d_c + d_p \\ 0 & \text{for } r \ge d_c + d_p \end{cases} \tag{6.27}$$

Furthermore, by a simple geometric consideration, it can be shown that effective triplet and higher-order many-body forces vanish provided the size ratio between colloids and polymers $q = d_p/d_c$ is smaller than 0.154. In this case, the AO model is formally equivalent to an effective one-component system with a short ranged attraction, which immediately opens the way for large-scale simulations.

The phase diagram of the AO model was explored by computer simulations on three different levels: first, one-component calculations using the effective pair potential (6.27) have been performed [69], which are exact for $q < 0.154$. Secondly, more recently, Dijkstra has simulated the full effective Hamiltonian including effective many-body forces to arbitrary order for $q = 1$ [70]. Finally, brute force simulation with explicit ideal-gas polymers have been carried out [71]. The emerging phase diagram involves three phases: gas (i.e. colloidal poor), liquid (i.e. colloidal rich) and an fcc colloidal crystal. A liquid phase is stable if the ratio q is larger than $q_c \approx 0.5$.

On the other hand, theoretical progress was made by constructing a free volume theory for the fluid bulk free energies [72] which provides a reliable

estimate for the gas-liquid transition. A free-energy density functional for the AO colloid-polymer mixtures, valid for arbitrary inhomogeneous situations, was constructed [73] in the spirit of Rosenfeld's fundamental measure approach [74], which reproduces the effective interaction (6.27) for a colloid pair and the free volume theory of Ref. [72]. This density functional was applied to wetting phenomena of planar walls. A novel type of wetting involving growth of only few colloidal liquid layers on top of the wall as liquid-gas coexistence is approached was predicted by density functional theory [75] and confirmed by computer simulations [70,71]. This wetting scenario only shows up for ratios larger than q_c, so that one can speculate that it is produced by the intrinsic many-body nature of the effective forces.

Obviously, the AO model has the short-coming of idealized interactions. More realistic models involve a non-zero polymer-polymer interaction and a softer polymer-wall interaction [76]. On the other hand, full two-component simulations of colloids and polymers were performed [77,78] where the polymers are defined on a lattice. Clearly these include any effective many-body interactions. A second computationally less demanding technique is to calculate effective pair interactions between a colloid and a polymer first by a monomer-resolved reference simulation. This strategy was followed in the more general context of mixtures of colloids and star polymers for small size ratios q. Supported by theoretical scaling arguments the following pair interaction between a hard-sphere colloid and a star polymer was obtained [79,47]:

$$v_{cp}(r) = k_B T \Lambda f^{3/2} \left(\frac{d_c}{2r+d_c}\right) \tag{6.28}$$

$$\times \begin{cases} -\ln(\frac{2r-d_c}{\sigma}) + (\frac{(2r-d_c)^2}{\sigma^2} - 1)((1+4\kappa)/(1+2\kappa)) + \zeta & \text{for } r \le \frac{d_c+\sigma}{2}; \\ \zeta\, \mathrm{erfc}(\kappa(2r-d_c)/\sigma)/\mathrm{erfc}(\kappa) & \text{else,} \end{cases}$$

Here, Λ and κ are known parameters depending on the functionality f of the star, $\zeta = \sqrt{\pi}\mathrm{erfc}(\kappa)\exp(\kappa^2)/(\kappa(1+2\kappa^2))$, σ denotes the corona diameter of the star and $\mathrm{erfc}(x)$ is the complementary error function. For $r \to d_c/2$ the potential diverges logarithmically as for the star-star interaction (6.23). Linear polymer chains are obtained as the special case $f = 2$ where $\Lambda = 0.46$ and $\kappa = 0.58$. The two-component system with effective pair interactions was investigated in detail by further simulation and liquid integral equation theory. For different arm numbers f, the fluid-fluid demixing transition was calculated [79] in good agreement with experimental data. Furthermore, the freezing transitions was discussed. Above a critical arm number of $f_c \approx 10$, fluid-fluid demixing was preempted by freezing [80].

In case of polymer size comparable or larger than the colloidal diameter d_c, effective many-body forces play a significant role. Complementary methods such as monomer-resolved liquid intergral equations methods combined with the PRISM approach [81] or field-theoretic calculations [82] have provided

valuable insight into the structure of colloid-polymer mixtures. The limit of large q contains completely different physics, since the colloidal spheres represent then small perturbations for the long polymer chains [78].

6.8 Binary Colloidal "Alloys"

Binary mixtures of large and small sterically-stabilized colloids exhibit many unexpected phases. Such a binary colloidal "alloy" can be modelled as a two-component hard sphere system involving two colloidal diameters d_1 and d_2 ($d_2 < d_1$). If the size ratio $q = d_2/d_1$ is larger than 0.4, a large variety of stable phases involving different superlattice crystals are predicted by theory [83] and simulation [84] and observed experimentally [85] . We shall focus here more on the case of small q, where a depletion picture, similar to that discussed for colloid and polymer mixtures, should hold. In contrast to the AO-model, however, many-body forces are present for any q in the hard sphere mixture, but these can be shown to be small with respect to the pairwise contribution [9,11].

The effective depletion potential $v(r)$ between a pair of big spheres in a sea of small spheres has been efficiently calculated and analytically parameterized, based on the procedure of Roth et al. [10] as applied to the two-component hard sphere density functional of Rosenfeld [74]. As a function of r, $v(r)$ involves a short-ranged attraction followed by an oscillatory behaviour decaying exponentially with the bulk correlation length of the small spheres. The density functional predictions were confirmed by computer simulations [86,87] and by experiments [88].

One key question addressed during the last decade was whether the depletion attraction is strong enough to drive fluid-fluid phase separation (for a recent review see [24]). The problem was finally solved by computer simulation using the effective one-component model with the depletion pair potential [89,90]: a fluid-fluid demixing is obtained for $q < 0.1$ but this is always metastable with respect to the freezing transition into an fcc solid made up by the big spheres. The simulations of the effective one-component model were confirmed by full simulations of the true binary system [89] showing once more that the influence of triplet forces is negligible [9,11]. Simulation results for the phase diagram, as presented in terms of the packing fractions $\eta_1 = \pi\rho_1 d_1^3/6$ of the big particles and η_2^r of a reservoir of small particles in coexistence with the whole system, are shown in Fig. 6.3 for $q = 0.2, 0.1, 0.05$. Besides the fluid-fluid demixing which remains metastable, an isostructural solid-solid transition occurs at high η_1 for $q < 0.05$, as familiar for one-component systems with a short-ranged attraction [91,92]. As q decreases, the fluid-solid coexistence line becomes more and more horizontal until the sticky hard-sphere limit ($q \to 0^+$) is achieved where a vacuum coexists with a close-packed crystal. This example shows again that the effective interaction

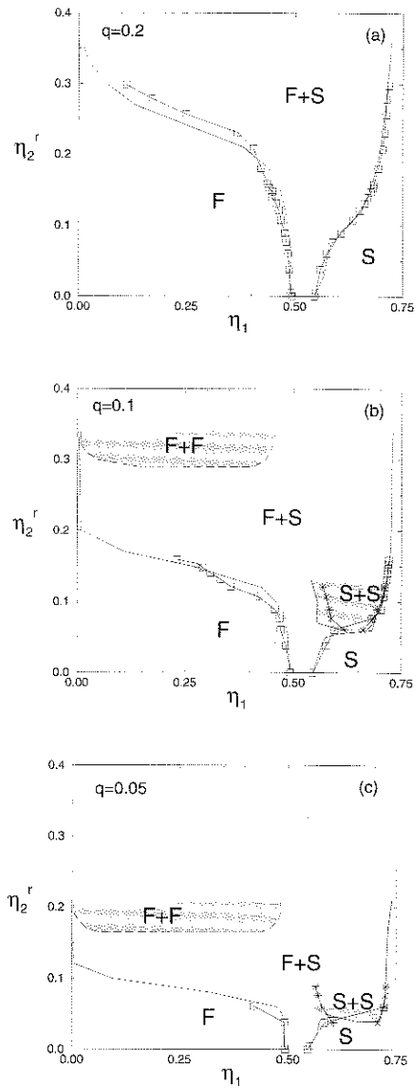

Fig. 6.3. Phase diagram of binary hard-sphere mixtures with size ratios (a) $q = 0.2$, (b) $q = 0.1$, and (c) $q = 0.05$ as a function of the large-sphere packing fraction η_1 and the small-sphere reservoir packing fraction η_2^r. F and S denote the stable fluid and solid (fcc) phase. $F + S$, $F + F$, and $S + S$ denote, respectively, the stable fluid-solid, the metastable fluid-fluid, and the (meta)stable solid-solid coexistence regions. The solid and dashed lines are the effective one-component results; the squares and the asterisks (joined by lines to guide the eye) denote, respectively, the fluid-solid and the solid-solid transition obtained from direct simulations of the true binary mixtures. Reproduced from Ref. [89] with permission.

picture allows qualitative and quantitative understanding of the topology of phase diagrams.

Further current research is focused on the sensitivity of the depletion potential to polydispersity of the small particles [93], and to small-small and big-small interactions beyond the hard sphere model [94]. Polydispersity smears out the oscillatory behaviour, while keeping the deep attraction near contact unchanged. Different small-small and big-small interaction have a significant impact on the effective big-big interaction: for instance, an attraction between the small particles or the big and small particles leads to repulsive effective interactions due to an accumulation of small particles on the surfaces of the big ones. This "inverse depletion effect" may be called accumulation repulsion. These recent findings imply that the effective interactions can be systematically tuned via the basic interactions and polydispersity.

6.9 From Colloidal to Nanoscales

Although the concept of effective interactions as described in Sect. 6.2 is exact in principle, there are limitations in applying it in practice. These limitations become more and more important if one considers smaller and smaller macroparticles, such that molecular details become more relevant. In fact, on nanoscales, chemical specificity is starting to become crucial, resulting in many different phenomena like solvation effects, hydration, hydrophilicity, hydrophobicity, forces determined by chemical bonding etc. In fact, these effects are essential to explain the structure and function of biological macromolecules in solution, e.g. of proteins. Under these circumstances, it is clear that one cannot get away with relatively simple effective interactions, characterized by few parameters, like those discussed previously in the context of colloidal length scales. The immediate question arising is when and where does the simple coarse-graining concept break down if one crosses over from the colloidal to the nanoscale. Basically there are *two major caveats*: The first concerns the choice of the microscopic degrees of freedom which are to be integrated out; the second concerns internal degrees of freedom and modelling of the big particles themselves. In the sequel we shall discuss these two points in detail and illustrate them using two examples.

Regarding the first point, even on nanoscales there remains an enormous number of microscopic degrees of freedom. The relevant question is which of these have to be included explicitly in the starting Hamiltonian or may be ignored or replaced by effective parameters. This is a tricky question when length scales are less clearly separated than in colloidal systems. For long polymer chains, scaling theory implies that molecular details are unimportant for most purposes, such that one can get away with simple lattice models (as discussed for linear polymer chains) or with a simple monomeric description of beads (as discussed for star polymers). For charged colloids, in the primitive approach, the solvent molecules are not considered explicitly but

only enter via the dielectric constant. The charged microions, on the other hand, are included explicitly, since their Coulomb interaction is stronger than the dipolar forces acting between the solvent. While this seems to be justified for micron-sized colloidal particles with typical interparticle spacing of microns (provided molecular details on the colloidal surface are encaptured by an effective colloidal charge), it is questionable when the colloidal diameter or the intercolloidal distance is becoming comparable to the correlation lenth or interaction range of the microcopic degrees of freedom, i.e. for nanoparticles.

As an illustration, we consider the effective interaction between two nano-sized charged colloidal particles in a *hard sphere solvent*. A systematic comparison between primitive-model calculations where the solvent is neglected and the full system including the hard sphere solvent was performed recently by Allahyarov and one of us [95,87]. On an intermediate level, one can formally integrate out the solvent, ending up with effective interactions between the charged particles. If these are approximated to be pairwise, one obtains the so-called solvent averaged primitive model [96]. In this model, the interaction between charged species comprises the bare Coulomb interaction and the effective depletion interaction between hard spheres as discussed in Sect. 6.8. Extensive computer simulations [95,87] have shown that the total effective force between charged colloidal particles does depend on the presence of the discrete solvent. Even the sign of the effective interaction can be different in the primitive model as compared to the full solvent result. An example for divalent counterions and a charge asymmetry of $q_p : q_c = 64 : 2$ is shown in Fig. 6.4 where the ratio of the three hard-core diameters of colloidal particles, counterions and solvent particles is $d_p : d_c : d_s = 14 : 2 : 1$. In fact, interpreting the solvent size as a microscopic scale, the colloidal diameter is 14 times larger and thus falls into the nano-regime. While the primitive model reference calculations yield a repulsive effective force, the simulations including a hard-sphere solvent result in an attractive force.

The solvent-averaged primitive model, on the other hand, reproduces the data of the full solvent simulation rather well. The simulation time for the solvent-averaged primitive model is similar to that of the primitive model, since the number of particles simulated is the same, while the full simulation requires the inclusion of many solvent particles. Hence the concept of effective interactions as applied to the solvent degrees of freedom alone, makes simulations feasible in the spirit of McMillan-Mayer theory. But even more importantly, the solvent-averaged model also provides insight into the basic physics: the depletion attraction between a colloidal sphere and counterions favours an accumulation of the latter on the colloidal surfaces, thus enhancing the screening. It is this effect which, together with strong Coulomb correlations, leads to the attraction evident in Fig. 6.4 which is completely missing in the primitive model. For large colloidal spheres, on the other hand, it was shown in Ref. [87] that the effect of a discrete hard sphere solvent can completely be accounted for by taking a different (effective) colloidal charge as input in the

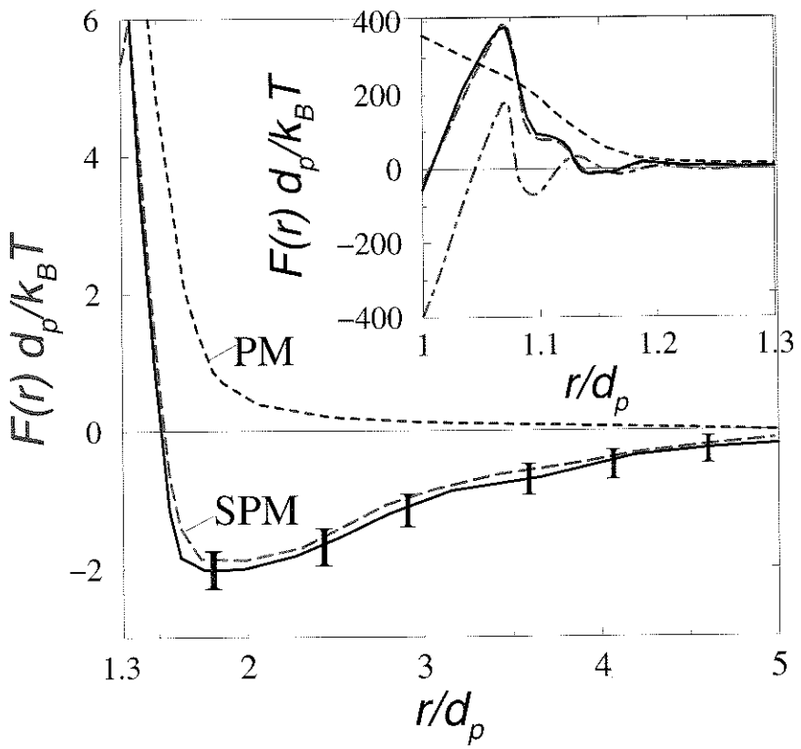

Fig. 6.4. Reduced distance-resolved force $F(r)d_p/k_BT$ versus reduced distance r/d_p between two charged colloids as obtained by computer simulations. The inset shows the same for nearly touching polyions of molecular distances. The parameters are: $q_c = 2$, $q_p = -64$, $d_p : d_c : d_s = 14 : 2 : 1$, $\epsilon = 81$, the volume fraction of the polyions in the periodically repeated box is $\eta_p = 5.8 \times 10^{-3}$. Solid line with error bars: full simulation including the hard sphere solvent; long-dashed line: solvent averaged primitive model; short-dashed line: primitive model; dot-dashed line in inset: solvent depletion force alone (for comparison).

primitive model calculations. Consequently simple coarse-graining is justified provided an effective colloidal charge is used.

The second caveat for coarse-graining concerns the description of the big colloidal particles. Up to now we have modelled them as homogeneously charged hard spheres in the context of charged suspensions. Coming down to nanoscales, the molecular details and internal degrees of freedom of the large particles themselves, which are neglected in statistical descriptions of colloidal dispersions, are becoming more and more relevant. We shall illustrate this using an example where the *discreteness of the charge pattern* on the colloidal surfaces turns out to be crucial provided the particles are nano-

sized. This is of particular importance for proteins which are characterized by nanoscale electrostatic patches.

In a recent computer simulation [97], the effective interaction between two nano-sized colloidal spheres (modelling globular proteins) with a discrete charge pattern was calculated within the primitive model as a function of added salt concentration. A snapshot of a protein pair is shown in Fig. 6.5. Discrete elementary point charges were placed on the protein surface with a finite depth. Consequently the effective interaction not only depends on the centre-to-centre distance r but also on the relative orientations of the two proteins. These represent additional statistical degrees of freedom associated with the macroparticles. The data were compared to the standard description with the charge uniformly smeared over the particle surface. A key quantity controlling protein crystallization [98] is the second osmotic virial coefficient B_2 which can readily be measured by scattering methods in dilute protein solutions. B_2 can be shown [97] to be related to the effective interaction by

$$B_2 = \frac{1}{2}\int d^3r[1 - \exp(-v(r)/k_BT)] \tag{6.29}$$

in formal analogy to the orientation-independent case of the smeared charged model. Here $v(r)$ is the integral of the canonical orientational average of the distance-resolved effective force projected onto the separation vector between the two proteins [97].

A detailed calculation of B_2 as a function of added salt reveals that it behaves non-monotonically as a function of added salt concentration, in agreement with several experimental studies [99]. This non-monotonicity, however, disappears when the surface charge uniformly smeared out. It can thus be traced back to strong Coulomb correlations induced by the discrete binding centers near the surface. This example shows that important effects are lost even qualitatively, when the coarse graining of nanoparticles is pushed too far.

6.10 Conclusions

In summary, we have demonstrated that the concept of effective interactions allows large-scale simulations and provides additional insight into the physical mechanisms governing colloidal dispersions and polymer solutions. We conclude with a discussion about multiple *time* scales in the context of colloidal dispersions.

The dynamics of colloidal particles embedded in a solvent involves many different time scales ranging from the collision time $\tau_s \approx 10^{-14} sec$ of the solvent molecules, over the relaxation time $\tau_B \approx 10^{-9} sec$ of the total colloid momentum and the propagation time $\tau_H \approx 10^{-9} sec$ of hydrodynamic interactions, to the Brownian time $\tau_0 \approx 10^{-6} sec$ on which diffusive motion of the

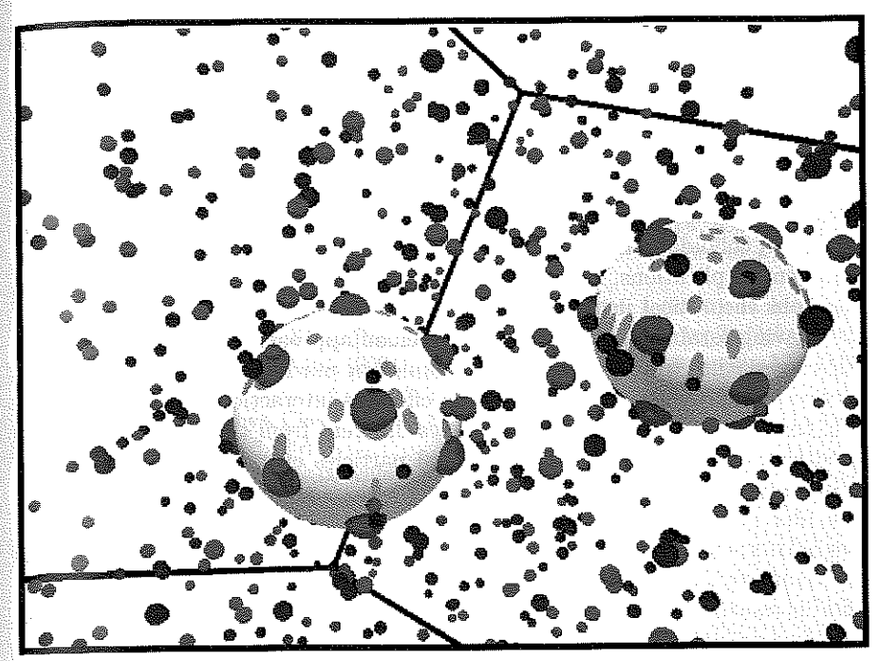

Fig. 6.5. Simulation snapshot of a microion configuration around two model proteins separated by $r = 1.7d_p$, d_p denoting the protein hard core diameter. The proteins carry 15 discrete charges e, monovalent salt molarity is $c_s = 0.206 Mol/\ell$. The globular protein molecules are shown as two large grey spheres. The embedded small dark spheres on their surface mimic the discrete protein charges. The small grey spheres are counterions, while the black spheres are coions.

colloidal particles is observed. Consequently there is almost complete time scale separation

$$\tau_s << \tau_B \simeq \tau_H << \tau_0. \tag{6.30}$$

It is a challenging question whether - in analogy with bridging length scale gaps - one can "integrate out" the fast dynamical processes which happen on the time scale τ_s in order to arrive at an "effective dynamics" on larger time scales. The traditional approach is a stochastic one, as embodied in Langevin and Fokker-Planck formulations [114,115], but a rigorous derivation of the Fokker-Planck equation from the initial full Liouville equation for dilute colloidal suspensions exposes the intrinsic limitations of the Fokker-Planck equation, due to the similarity of the time scales τ_B and τ_H [116]. Clearly a dynamical counterpart of the effective interaction concept governing the thermodynamics and statics is missing. From a simulation point of view however, relying on an (almost) complete time scale separation between solvent and colloidal dynamics, one typically describes the motion of

the colloidal particles by a completely overdamped Langevin equation with stochastic forces exerted onto the colloids modelling the random solvent kicks [100,101]. Within such a Brownian approach operating on a time scale τ_0, the hydrodynamic interactions act instantaneously. Much recent effort was spent to treat these hydrodynamic interactions approximatively [102] by using different computational schemes such as lattice-Boltzmann techniques [103], Stokesian Dynamics [104], dissipative particle dynamics [105], and fluidizing the solid colloidal particles [106]. Although these algorithms are powerful in different applications, it is fair to say that all of these approaches lack a rigorous theoretical justification.

Having established a stochastic Brownian approach for the colloidal particles resulting from the solvent dynamics, a much more modest question concerns the dynamical utility of the effective interaction concept originating from integrating out small particles different from the solvent (counter- and salt ions, polymers, small colloidal particles etc). One may conjecture that it is only in the case of a complete time scale separation between the big and small particle dynamics that the effective interaction has a true dynamical meaning. This is the reason why the effective interaction potential is frequently combined with Brownian dynamics simulations for the colloids. For instance, the effective DLVO-potential has been combined with Brownian dynamics simulations in order to investigate the glass transition [107], long-time self-diffusion [108], linear shear flow [109–111], and phase transitions in driven colloidal mixtures [112,113]. It would be very interesting to test and study systematically how far one can get with the coarse-graining approach as far as dynamical questions are concerned.

Acknowledgements

We thank E. Allahyarov, M. Dijkstra, J. Dzubiella, A. Jusufi, C. N. Likos, A. A. Louis and R. Pierre for help and for valuable comments.

References

1. V. Lobaskin, A. Lyubartsev, P. Linse, Phys. Rev. E **63**, 020401 (2001).
2. C. W. J. Beenakker, P. Mazur, Physica **126A**, 349 (1984).
3. See e.g R. van Roij, M. Dijkstra, J.P. Hansen, Phys. Rev. E **59**, 2010 (1999).
4. For an extensive review of classical DFT see R. Evans in "Fundamentals of Inhomogeneous Fluids", edited by D. Henderson (Marcel Decker, New York, 1992).
5. J. P. Hansen and E. Smargiassi, in "Monte Carlo and Molecular Dynamics of Condensed Matter Systems", edited by K. Binder and G. Ciccotti (Societa Italiana di Fisica, Bologna, 1996).
6. See e.g. G. Galli and M. Parrinello, in "Computer Simulations in Materials Science", P. 282, edited by M. Meyer and V. Pontikis (Kluwer, Dordrecht, 1991)

7. H. Löwen, J. P. Hansen, P. A. Madden, J. Chem. Phys. **98**, 3275 (1993).
8. F. Gygi, G. Galli, Phys. Rev. B **52**, R 2229 (1995).
9. S. Melchionna, J. P. Hansen, Phys. Chem. Chem. Phys. **2**, 3465 (2000).
10. R. Roth, R. Evans, S. Dietrich, Phys. Rev. E **62**, 5360 (2000).
11. D. Goulding, S. Melchionna, Phys. Rev. E **64**, 011403 (2001).
12. J. P. Hansen, H. Löwen, Ann. Rev. Phys. Chem. **51**, 209 (2000).
13. L. Belloni, J. Phys. Condens. Matter **12**, R549 (2000).
14. B. V. Derjaguin, L. D. Landau, Acta Physicochim. USSR **14**, 633 (1941); E. J. W. Verwey and J. T. G. Overbeek, *Theory of the Stability of Lyophobic Colloids*. (Elsevier, Amsterdam, 1948).
15. A. Delville, R. J. M. Pellenq, Molecular Simulation **24**, 1 (2000); R. Messina, C. Holm, K. Kremer, Phys. Rev. Lett. **85**, 872 (2000); T. Terao, T. Nakayama, Phys. Rev. E **63**, 041401 (2001); B. Hribar, V. Vlachy, Langmuir **17**, 2043 (2001).
16. A. Delville, J. Phys. Chem. B **103**, 8296 (1999); A. Delville, P. Levitz, J. Phys. Chem. B **105**, 663 (2001)
17. S. Meyer, P. Levitz, A. Delville, J. Phys. Chem. B **105**, 10684 (2001).
18. H. Löwen, E. Allahyarov, J. Phys.: Condensed Matter **10**, 4147 (1998).
19. R. D. Groot, J. Phys. **95**, 9191 (1991).
20. M. J. Stevens, M. L. Falk, M. O. Robbins, J. Chem. Phys. **104**, 5209 (1996).
21. H. Löwen, G. Kramposthuber, Europhys. Lett. **23**, 673 (1993).
22. H. Löwen, Phys. Rev. Lett. **72**, 424 (1994). J. Chem. Phys. **100**, 6738 (1994).
23. S. Kutter, J. P. Hansen, M. Sprik, E. Boek, J. Chem. Phys. **112**, 311 (2001).
24. M. Dijkstra, Current Opinion in Colloid and Interface Science **6**, 372 (2001).
25. For a review, see T. Tomasi , M. Perico, Chem. Rev. **94**, 2027 (1994).
26. M. Marchi, D. Borgis, N. Levy, P. Ballone, J. Chem. Phys. **114**, 4377 (2001).
27. D. M. York, M. Karplus, J. Phys. Chem. A **103**, 11060 (1999).
28. R. A. Marcus, J. Chem. Phys. **24**, 966, 979 (1956).
29. B. U. Felderhof, J. Chem. Phys. **67**, 493 (1977).
30. R. Allen, J. P. Hansen, S. Melchionna, Phys. Chem. Chem. Phys. **3**, 4177 (2001).
31. R. Allen, S. Melchionna, J. P. Hansen to be published.
32. C. Mischler, J. Baschnagel, K. Binder, Advances in Colloid and Interface Science **94**, 197 (2001).
33. P. J. Flory, W. R. Krigbaum, J. Chem. Phys **18**, 1086 (1950).
34. A. Y. Grosberg, P. G. Khalatur, A. R. Khokhlov, Makromol. Chem. Rapid Comm. **3**, 709 (1982).
35. J. Dautenhahn, C. K. Hall, Macromolecules **27**, 5399 (1994), and references therein.
36. A. A. Louis, P. G. Bolhuis, J. P. Hansen, E. J. Meijer, Phys. Rev Letters **85**, 2522 (2000) P. G. Bolhuis, A. A. Louis, J. P. Hansen, E. J. Meijer, J. Chem. Phys. **114**, 4296 (2001).
37. B. Krüger, L. Schäfer, A. Baumgärtner, J. Phys. (Paris) **50**, 319 (1989).
38. V. Krakoviack, A. A. Louis, J. P. Hansen, to be published.
39. C. H. Bennett, J. Comp. Phys. **22**, 245 (1976).
40. D. Frenkel, B. Smit, "Understanding Molecular Simulation", 2^d Edition (Academic Press, San Diego, 2001).
41. P. G. Bolhuis, A. A. Louis, J. P. Hansen, Phys. Rev. E **64**, 021801 (2001).
42. C. von Ferber, A. Jusufi, C. N. Likos, H. Löwen, M. Watzlawek, Europhys. Journal E **2**, 311 (2000).

43. See e.g. J. P. Hansen, I. R. McDonald, "Theory of Simple Liquids" 2^d edition (Academic Press, London, 1986).
44. A. A. Louis, P. G. Bolhuis, J. P. Hansen, Phys. Rev. E **62**, 7961 (2000).
45. C. N. Likos, Physics Reports **348**, 267 (2001).
46. R. L. Henderson, Phys. Lett. **49A**, 197 (1974).
47. A. Jusufi, J. Dzubiella, C. N. Likos, C. von Ferber, H. Löwen, J. Phys.: Condensed Matter **13** 6177 (2001).
48. A. A. Louis, P. G. Bolhuis, E. J. Meyer, J. P. Hansen, cond-mat (011518).
49. For a review see K. S. Schweizer, J. G. Curro, Adv. Chem. Phys. **98**, 1 (1997).
50. V. Krakoviack, J. P. Hansen, A. A. Louis, cond-mat / 0110387
51. For a review see: G. S. Grest, L. J. Fetters, J. S. Huang, D. Richter, Advances in Chemical Physics, Volume XCIV, 67 (1996)).
52. T. A. Witten, P. A. Pincus, Macromolecules **19**, 2509 (1986).
53. M. Daoud, J. P. Cotton, J. Phys. (Paris) **38**, 983 (1977).
54. C. N. Likos, H. Löwen, M. Watzlawek, B. Abbas, O. Jucknischke, J. Allgaier, D. Richter, Phys. Rev. Letters **80**, 4450 (1998).
55. A. Jusufi, M. Watzlawek, H. Löwen, Macromolecules **32**, 4470 (1999).
56. M. Watzlawek, C. N. Likos, H. Löwen, Phys. Rev. Letters. **82**, 5289 (1999).
57. M. Watzlawek, H. Löwen, C. N. Likos, J. Phys. Condensed Matter **10**, 8189 (1998).
58. G. A. McConnell, A. P. Gast, Macromolecules **30**, 435 (1997).
59. S. T. Milner, T. A. Witten, M. E. Cates, Macromolecules **21**, 2610 (1988).
60. J. Mewis, W. J. Frith, T. A. Strivens, W. B. Russel, A. I. Ch. E. J. **35**, 415 (1989).
61. U. Genz, B. D'Aguanno, J. Mewis, R. Klein, Langmuir **10**, 2206 (1994).
62. C. N. Likos, H. Löwen, A. Poppe, L. Willner, J. Roovers, B. Cubitt, D. Richter, Phys. Rev. E **58**, 6299 (1998).
63. A. Jusufi, C. N. Likos, H. Löwen, Phys. Rev. Letters (in press).
64. P. Pincus, Macromolecules **24**, 2912 (1991).
65. C. N. Likos, M. Schmidt, H. Löwen, M. Ballauff, D. Pötschke, P. Lindner, Macromolecules **34**, 2914 (2001).
66. C. N. Likos, private communication.
67. A. Lang, C. N. Likos, M. Watzlawek, H. Löwen, J. Phys. Condensed Matter **12**, 5087 (2000).
68. S. Asakura, F. Oosawa, J. Chem. Phys. **22**, 1255 (1954).
69. M. Dijkstra, J. M. Brader, R. Evans, J. Phys.: Condensed Matter **11**, 10079 (1999).
70. M. Dijkstra, to be published.
71. I. Götze, Diploma Thesis, University of Düsseldorf, 2002.
72. H. N. W. Lekkerkerker, W. C. K. Poon, P. N. Pusey, A. Stroobants, P. B. Warren, Europhys. Lett. **20**, 559 (1992).
73. M. Schmidt, H. Löwen, J. M. Brader, R. Evans, Phys. Rev. Letters **85**, 1934 (2000).
74. Y. Rosenfeld, M. Schmidt, H. Löwen, P. Tarazona, Phys. Rev. E **55**, 4245 (1997).
75. M. Schmidt, H. Löwen, J. M. Brader, R. Evans, J. Phys.: Condensed Matter **14**, L1 (2002).
76. A. A. Louis, R. Finken, J. P. Hansen, Phys. Rev. E **61**, R1028 (2000).
77. E. J. Meijer, D. Frenkel, Physica A **213**, 130 (1995).

78. A. Johner, J. F. Joanny, S. Diez Orrite, J. BonetAvalos, Europhys. Letters **56**, 549 (2001).
79. J. Dzubiella, A. Jusufi, C. N. Likos, C. von Ferber, H. Löwen, J. Stellbrink, J. Allgaier, D. Richter, A. B. Schofield, P. A. Smith, W. C. K. Poon, P. N. Pusey, Phys. Rev. E **64**, 01040 (2001).
80. J. Dzubiella, C. N. Likos, H. Löwen, to be published.
81. M. Fuchs, K. S. Schweizer, Phys. Rev. E **64**, 021514 (2001).
82. A. Hanke, E. Eisenriegler, S. Dietrich, Phys. Rev. E **59**, 6853 (1999).
83. H. Xu, M. Baus, J. Phys.: Condensed Matter **4**, L663 (1992).
84. M. D. Eldridge, P. A. Madden, D. Frenkel, Mol. Phys. **79**, 105 (1993).
85. P. Bartlett, R. H. Ottewill, P. N. Pusey, Phys. Rev. Lett. **68**, 3801 (1992).
86. R. Dickman, P. Attard, V. Simonian, J. Chem. Phys. **107**, 205 (1997).
87. E. Allahyarov, H. Löwen, Phys. Rev. E **63**, 041403 (2001).
88. J. C. Crocker, J. A. Matteo, A. D. Dinsmore, A. G. Yodh, Phys. Rev. Letters **82**, 4352 (1999).
89. M. Dijkstra, R. van Roij, R. Evans, Phys. Rev. E **59**, 5744 (1999).
90. N. G. Almarza, E. Enciso, Phys. Rev. E **59**, 4426 (1999).
91. P. Bolhuis, M. Hagen, D. Frenkel, Phys. Rev. E **50**, 4880 (1994).
92. C. N. Likos, Z. T. Németh, H. Löwen, J. Phys. Condensed Matter **6**, 10965 (1994).
93. D. Goulding, J. P. Hansen, Mol. Phys. **99**, 865 (2001).
94. A. A. Louis, R. Roth, E. Allahyarov, H. Löwen, to be published.
95. E. Allahyarov, H. Löwen, J. Phys. Condensed Matter **13**, L277 (2001).
96. H. Löwen, E. Allahyarov, J. Dzubiella, C. von Ferber, A. Jusufi, C. N. Likos, M. Heni, Philos. Trans. R. Soc. Lond. A **359**, 909 (2001).
97. E. Allahyarov, H. Löwen, A. A. Louis, J. P. Hansen, *Discrete charge patterns, Coulomb correlations and interactions in protein solutions,* Europhys. Letters (in press).
98. A. George, W. W. Wilson, Acta Cryst. D **50**, 361 (1994); G. A. Vliegenthart, H. N. W. Lekkerkerker, J. Chem. Phys. **112**, 5364 (2000).
99. B. Guo, S. Kao, H. McDonald, A. Asanov, L. L. Combs, W. W. Wilson, J. Cryst. Growth **196**, 424 (1999); D. N. Petsev, B. R. Thomas, S. T. Yau, P. G. Vekilov, Biophysical Journal **78**, 2060 (2000).
100. For a review, see P. N. Pusey, in "Liquids, Freezing and the Glass Transition", edited by J. P. Hansen, D. Levesque and J. Zinn-Justin (North Holland, Amsterdam, 1991).
101. J. K. G. Dhont, "An Introduction to Dynamics of Colloids", Elsevier, Amsterdam, 1996.
102. G. Nägele, Physics Reports, **272**, 215 (1996).
103. A. J. C. Ladd, R. Verberg, J. Stat. Phys. **104**, 1191 (2001).
104. See e.g.: R. Pesché, G. Nägele, Europhys. Lett. **51**, 584 (2000); H. M. Schaink, P. A. Nommensen, R. J. J. Jongschaap, J. Mellema, J. Chem. Phys. **113**, 2484 (2000).
105. P. B. Warren, Current Opinion in Colloid and Interface Science **3**, 620 (1998).
106. H. Tanaka, T. Araki, Phys. Rev. Lett. **85**, 1338 (2000).
107. H. Löwen, J. P. Hansen, J. N. Roux, Phys. Rev. A **44**, 1169 (1991).
108. H. Löwen, G. Szamel, J. Phys. Condensed Matter **5**, 2295 (1993).
109. S. Butler, P. Harrowell, J. Chem. Phys. **103**, 4653 (1995); J. Chem. Phys. **105**, 605 (1996).

110. S. R. Rastogi, N. Wagner, S. R. Lustig, J. Chem. Phys. **104**, 9234 (1996).
111. N. Olivi-Tran, R. Botet, B. Cabane, Phys. Rev. E **57**, 1997 (1998).
112. H. Löwen, G. Hoffmann, Phys. Rev. E **60**, 3009 (1999).
113. J. Dzubiella, G. P. Hoffmann, H. Löwen, *Lane formation in binary colloidal mixtures driven by an external field,* Phys. Rev. E (in press).
114. N. G. van Kampen, "Stochastic Processes in Physics and Chemistry (North Holland, Amsterdam, 1990).
115. W. Hess and R. Klein, Adv. Phys. **32**, 173 (1983).
116. For a review, see L. Bocquet and J. P. Hansen, in "Dynamics: Models and Kinetic Methods for Non-Equilibrium Many-Body Systems", edited by J. Karkheck (Kluwer Academic, Dordrecht, 2000).